Bull. Mater. Sci. (2019) 42:165
https://doi.org/10.1007/s12034-019-1847-8
© Indian Academy of Sciences

A detailed parametric study on the operating frequency of chloride ion-electrically charged carbon nanotube oscillators

F SADEGHI[1,2,*] and R ANSARI[1]
[1]Department of Mechanical Engineering, University of Guilan, PO Box 3756, Rasht, Iran
[2]Department of Engineering Sciences, Sabalan University of Advanced Technologies (SUAT), Namin, Iran
*Author for correspondence (Fatemeh_sadeghi_64@yahoo.com)

MS received 12 October 2018; accepted 2 January 2019; published online 21 May 2019

Abstract. Fabrication of new types of nanoscale oscillators with enhanced operating frequency has become the focal centre of interest. The aim of this paper is to explore the mechanical oscillatory behaviour of chloride ion tunnelling through carbon nanotubes (CNTs) decorated with identical functional groups at both ends. To this end, our previously proposed analytical expression for total potential energy between an ion and a functionalized CNT is used to derive a new semi-analytical expression for the accurate evaluation of oscillation frequency. With respect to the proposed frequency formula obtained from the conservation of mechanical energy principle, a comprehensive study is conducted to gain an insight into the effects of different parameters such as, sign and magnitude of functional group charge, nanotube length and initial conditions on the operating frequency of chloride ion-electrically charged CNT oscillators. It is revealed that the presence of functional groups, especially ones with the opposite charges to the chloride ion, leads to enhancement of the maximum achievable frequency. It is further observed that optimal frequency is attained when the ion oscillates near the ends of a positively charged nanotube.

Keywords. Chloride ion; carbon nanotubes; functional groups; oscillation frequency.

1. Introduction

Carbon nanotubes (CNTs) exhibiting many superior electrical, mechanical and thermal properties have wide prospects as constituents in nanoelectromechanical systems (NEMS) [1,2]. Up to now, various types of molecular devices based on CNTs have been proposed, amongst them nanomechanical oscillators have received considerable attention from the nanotechnology community. This is mainly attributed to the exceptional ability of these nano-devices to generate frequencies in the gigahertz (GHz) range which has been far beyond the ability of micro-oscillators. Nano-oscillators, or the so-called GHz oscillators, might have many potential applications, such as ultra-fast optical filters and ultra-sensitive nanoantenne and they can also be applied to nanoscale actuators, sensors, resonators, filters, motors and switching devices [3–5]. So far, different types of nanomechanical oscillators have been proposed in the published literature [6–9] and there have been continuing efforts towards fabricating novel ultra-high frequency nano-oscillators.

A breakthrough in the area of nano-oscillators was made by Cumings and Zettl [10] who declared that controlled and reversible telescopic extension of multi-walled carbon nanotubes (MWCNTs) is feasible. In their experiment, it was observed that as the core tube is pulled out and set free, it spontaneously pulls back into the housing shell owing to the restoring force caused by the van der Waals (vdW) interatomic interaction acting on the core tube. This experiment led to the suggestion that double-walled carbon nanotubes (DWCNTs) could be utilized as 0.1–1 GHz oscillators. Zheng and Jiang [11] then employed a continuum approximation of discrete atoms, which theoretically estimated that these nano-oscillators can have frequencies far beyond 1 GHz. Zheng *et al* [12] also reported the negligible effect of frictional forces on the oscillation frequency of nested CNT oscillators. The results of these studies have profound implications for research workers to fabricate different types of nanomechanical oscillators with operating frequencies in the GHz range. Nano-oscillators presently manufactured in experimental investigations are close to or already on the verge of quantum limit [13]. These devices may be viewed as quantum-mechanical oscillators when operating at several GHz and ultra-low temperatures [14]. To capture quantum effects in such devices, a fully quantum-mechanical treatment is required. Fock states, which are difficult to create, are used to describe quantum dynamics in nano-oscillators [15]. Indeed, excitations of oscillatory systems usually lead to the production of thermal states or coherent states instead of quantum Fock states. However, quantum oscillatory states can be prepared through coupling oscillators to atomistic systems [15]. The reader is referred to refs [16,17] for more details about quantum effects on nano-oscillators.

In many atomistic studies, molecular dynamics (MD) simulations have been extensively employed to predict the

performance of high-frequency CNT oscillators [18–22]. In this regard, Legoas *et al* [23,24] suggested that the oscillation frequency of nested CNT oscillators is sensitive to the configurations of inner and outer tubes. Rivera *et al* [25,26] investigated the damping effects of oscillatory motion. Liu *et al* [27] revealed that the oscillation frequency of MWCNTs can be tuned by the length of the outer nanotube. Coluci *et al* [28] exhibited chaotic signatures in the motion of coupled CNT oscillators. Song and Zha [29] examined the effects of radius and vacancy defect of single-walled carbon nanotubes (SWCNTs) on the oscillatory behaviours of C_{60}-nanotube oscillators. Ansari *et al* [30] performed MD simulations to examine the effect of electric charges on the operation of ion-based CNT oscillators. Their results demonstrated that the use of electrically charged nanostructures instead of uncharged ones enhances the oscillation frequency, especially, when the core and shell are oppositely charged. Using the classical MD simulations, the issues of frictional forces and energy dissipation have also been widely studied in the literature [31–33].

Despite the reliability of MD-based models in the study of nanomaterials, their main drawback is that they are computationally inefficient especially, in the case of large atoms for simulation. Moreover, analytical expressions cannot be derived in these models because their computations are performed completely in a numerical way. As an alternative to MD-based models, one can utilize the continuum approximation of discrete atoms in which a discrete atomic structure can be replaced with a uniform distribution of atoms over the surface or the volume of molecules [34]. This approximation enables arriving at analytical or semi-analytical expressions for the vdW interactions of various nanodevices [35,36]. Girifalco [37] first employed the continuum approximation to evaluate the vdW interactions between two C_{60} molecules and then in cooperation with his colleagues, reported the successful application of this approximation to different forms of molecular systems [38–40]. The continuum approximation has been extensively adopted to study different issues, such as encapsulation of drug molecules inside CNTs [41], storage of lithium ions between graphene sheets [42], transportation of water molecules inside ultra-small CNTs [43] and relative motion of certain nanostructures [44]. In the framework of a continuum Lennard-Jones (LJ) model, Zavalniuk and Marchenko [45] presented explicit expressions for the longitudinal rigidities and frequencies of small- and large-amplitude telescopic oscillations of DWCNT and MWCNT and found that the predicted frequencies agree well with experimental data and numerical simulations. They also estimated the contribution of small-amplitude telescopic oscillations to the low-temperature specific heat of nanotubes. Using the continuum approximation in conjunction with the standard 6-12 LJ potential and neglecting the frictional forces, analytical expressions were presented for the vdW interactions and the oscillation frequency of CNT-based oscillators, such as CNT–CNT, C_{60}-CNT, CNT–CNT bundle and C_{60}-CNT bundle oscillators [46–48]. The oscillation frequencies of such nano-oscillators were obtained based on the simplifying assumption of vdW interaction force. To accurately model the dynamics of such nanodevices, however, Ansari *et al* [49–52] abandoned this assumption and proposed semi-analytical frequency statements using the conservation of mechanical energy principle. Based on their proposed frequency expressions, which were dependent on the system parameters, some new features of such oscillatory systems were revealed.

Reviewing the literature indicates that the issue of interacting ions with CNTs has been received considerable attention. Based on the first-principles calculations, Zubair *et al* [53] reported that iodine molecules in contact with a CNT interact to form monoiodide or/and polyiodide from two and three iodine molecules due to removal of electrons from the nanotube. Chan and Hill [54] employed applied mathematical modelling to study the transportation of sodium and chloride ions inside functionalized CNTs and determined the transportation time of an intruding ion through the nanotube. Recently, we also studied the mechanics of a chloride ion inside CNTs decorated with identical functional groups at both the ends [55]. Using the continuum approach and neglecting the quantum effects, we extracted analytical expressions to evaluate vdW interactions between the ion and CNT and electrostatic interactions between the ion and the two functional groups. Moreover, neglecting the frictional forces, the equation of motion was solved numerically to determine the time history of displacement and velocity of the ion. In this paper, using the analytical expression for total potential energy given in ref. [55], a semi-analytical expression based on the conservation of the mechanical energy principle is derived which accurately evaluates the oscillation frequency of the system. A comparison is also made between the oscillation frequency results generated from the equation of motion and energy equation. The distinctive feature of the proposed frequency formula is having a quick answer which enables us to thoroughly investigate the oscillation frequency of ion-based CNT oscillators under different system parameters including sign and magnitude of functional group charge, nanotube length and initial conditions.

2. Interactions between an ion and an electrically charged CNT

The geometry of an ion tunnelling through a positively charged CNT is shown in figure 1. As depicted, the origin of the Cartesian coordinate system (x, y, z) is situated at the middle of the nanotube of radius R_c and length $2L$ and Z is the location of ion measured from the origin. Furthermore, the charge of the ion and the total charge of each functional group are symbolized by q and Q, respectively. Following our previously published work, the total potential energy of the system can be written as [55]:

$$E^{(\mathrm{tot})}(Z) = E^{(\mathrm{vdW})}(Z) + E^{(\mathrm{elec})}(Z), \tag{1}$$

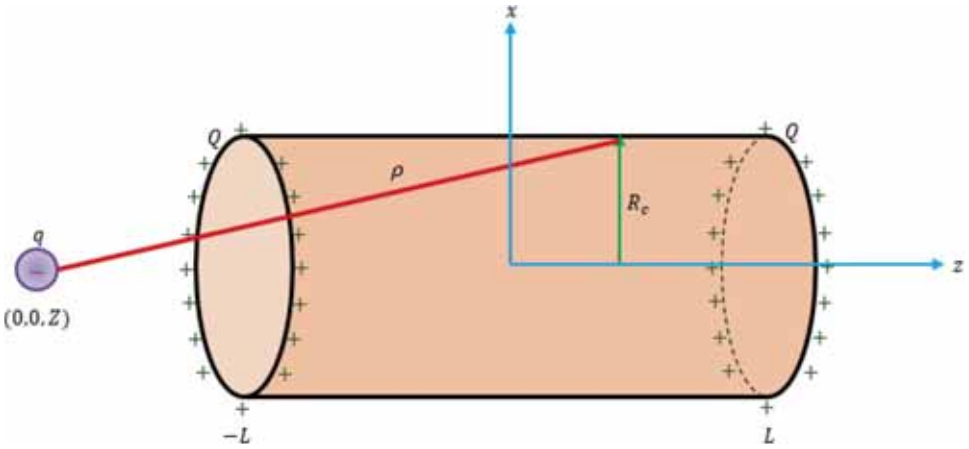

Figure 1. Geometry of the chloride ion interacting with a positively charged CNT.

in which $E^{(\mathrm{vdW})}$ is the vdW potential energy between the ion and CNT and $E^{(\mathrm{elec})}$ is the electrostatic potential energy between the ion and the two functional groups. Using a continuum approach, we derived the following analytical expression for the vdW potential energy [55]:

$$E^{(\mathrm{vdW})}(Z) = \sum_{n=1}^{2}(-1)^{n+1} \times \left(G_1 \tan^{-1}\vartheta_n + \sum_{i=1}^{5} G_{2i-1}\frac{\vartheta_n}{\left(1+\vartheta_n^2\right)^i}\right). \quad (2)$$

In equation (2), $\vartheta_n = Z_n/R_c$; $Z_1 = Z+L$ and $Z_2 = Z-L$. The constant parameters defined in this equation are also given by:

$$\begin{cases} G_1 = \frac{3}{8}\mu_1 + \frac{63}{256}\mu_2, \\ G_3 = \frac{1}{4}\mu_1 + \frac{21}{128}\mu_2, \\ G_5 = \frac{21}{160}\mu_2, \\ G_7 = \frac{9}{80}\mu_2, \\ G_9 = \frac{1}{10}\mu_2. \end{cases} \quad (3)$$

In the prior equation, $\mu_n = C_n R_c^{2-6n}$; $C_1 = -2\pi\eta_c A$ and $C_2 = 2\pi\eta_c B$, where A, B and η_c denote the attractive constant, the repulsive constant and the mean atomic surface density of the CNT, respectively.

Based on a continuum method, the electrostatic potential energy was also derived as [55]:

$$E^{(\mathrm{elec})}(Z) = \sum_{n=1}^{2}\frac{kqQZ_n}{\sqrt{R_c^2+Z_n^2}}, \quad (4)$$

where $k = 1/4\pi\varepsilon_0$ signifies the Coulomb constant in which ε_0 is the permittivity constant.

Moreover, upon differentiating the total potential energy with respect to Z due to the symmetry of the problem, the axial interaction force exerted on the ion was determined as follows [55]:

$$F_z^{(\mathrm{tot})}(Z) = -\frac{\mathrm{d}E^{(\mathrm{tot})}(Z)}{\mathrm{d}Z} = \sum_{n=1}^{2}\left(\frac{(-1)^n}{R_c}\left(\frac{G_1}{1+\vartheta_n^2} + \sum_{i=1}^{5} G_{2i-1}\frac{1-(2i-1)\vartheta_n^2}{\left(1+\vartheta_n^2\right)^{i+1}}\right) + \frac{kqQZ_n}{\left(R_c^2+Z_n^2\right)^{1.5}}\right). \quad (5)$$

For the geometrical parameters given in our recent published work [55], the results of total potential energy and interaction force related to uncharged, negatively charged and positively charged CNTs are reproduced and shown in figure 2a and b, respectively. The values of parameters needed for numerical evaluations are listed in table 1. The non-dimensional parameter C introduced in this figure is defined as the ratio of functional group charge to the magnitude of chloride ion charge, i.e., $C = Q/|q|$. As noted in ref. [55] and shown in figure 2, the overall shapes of total interactions are highly affected by the sign and value of the parameter C. For negatively/positively charged CNTs, the potential energy profile has two local maxima/minima near both ends of the nanotube and one local minimum/maximum at the middle length of the nanotube. Moreover, at this location, the vdW force is zero and the electrostatic forces between the ion and both functional groups have the same values, but reverse directions leading to vanishing of the total interaction force. In accordance with this figure, when the ion comes towards the non-zero extremum locations from the outside of negatively/positively charged CNTs, the total interaction force is repulsive/attractive and its direction is reversed as the ion passes each extremum location. According to what was discussed in ref. [55], based on the total potential energy profile, one can distinguish one oscillatory zone in the cases of

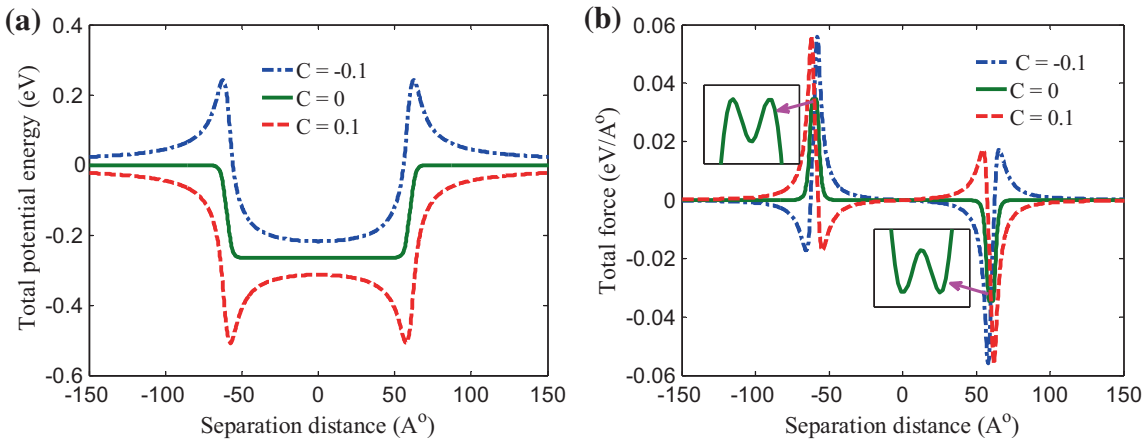

Figure 2. **(a)** Potential energy and **(b)** interaction force distribution related to uncharged, negatively charged and positively charged CNTs $(L = 60\,\text{Å})$.

Table 1. Constant values required for numerical evaluations [55].

Description	Parameter	Value
Radius of CNT	R_c	4.4695 Å
Mass of chloride ion	m_I	5.8872×10^{-26} kg
Attractive constant chloride ion-CNT	A	62.57 eV Å^6
Repulsive constant chloride ion-CNT	B	304015.33 eV Å^{12}
Number density of CNT	η_c	0.3812 Å^{-2}
Chloride ion charge	q	-1.602×10^{-19} C
Coulomb constant	k	8.99×10^9 Nm^2 C^{-2}

negatively charged and uncharged CNTs and two oscillatory zones in the case of positively charged CNTs. As mentioned, in the absence of functional groups, the preferred position of the system with respect to which inner core oscillates always occurs at the middle length of the nanotube. The preferred position related to negatively charged CNTs is also identical to that of uncharged ones on the condition that the initial separation distance does not exceed the local maximum location. Furthermore, for positively charged CNTs, the preferred position corresponding to the first oscillatory zone occurs near the local minimum location, whereas that corresponding to the second oscillatory zone occurs at the middle length of the nanotube. In this case, the two oscillatory zones overlap at a position outside the nanotube in which the total potential energy is equal to that at the middle length of the nanotube.

3. Frequency of oscillation

Since the frictional forces can be ignored in the oscillatory motion [12], the total potential energy remains constant. Accordingly, conservation of mechanical energy yields:

$$\frac{1}{2}m_I\left(\frac{dZ}{dt}\right)^2 + E^{(tot)}(Z) = E^{(tot)}(A_0) \Longrightarrow \int_0^{T/2} dt = \sqrt{\frac{m_I}{2}}\int_{2Z^*-A_0}^{A_0} \frac{dZ}{\sqrt{E^{(tot)}(A_0) - E^{(tot)}(Z)}}, \tag{6}$$

in which m_I, A_0 and T denote the mass of ion, motion amplitude and period of motion, respectively. In addition, Z^* signifies the preferred position of the system with respect to which the ion oscillates.

Integrating equation (6) with respect to time gives:

$$T = \alpha\sqrt{2m_I}\int_\beta^{A_0} \frac{dZ}{\sqrt{E^{(tot)}(A_0) - E^{(tot)}(Z)}}, \tag{7}$$

where

$$\alpha = \begin{cases} 2 & Z^* = 0 \\ 1 & Z^* \neq 0 \end{cases}, \quad \beta = \begin{cases} 0 & Z^* = 0 \\ 2Z^* - A_0 & Z^* \neq 0 \end{cases}. \tag{8}$$

The period of motion can be attained through performing the integral of equation (7) in a numerical way. This integral, however, has a singularity at the amplitude of motion which must be removed before performing the numerical integration. To do this, equation (7) is first divided into two terms as follows:

$$T_1 = \alpha\sqrt{2m_I}\int_\beta^{\delta A_0} \frac{dZ}{\sqrt{E^{(tot)}(A_0) - E^{(tot)}(Z)}}, \tag{9a}$$

$$T_2 = \alpha\sqrt{2m_I}\int_{\delta A_0}^{A_0} \frac{dZ}{\sqrt{E^{(tot)}(A_0) - E^{(tot)}(Z)}}, \tag{9b}$$

in which T_1 contains a non-singular integral, while T_2 contains a singular integral. Furthermore, δ is arbitrarily taken as 0.99.

Thereafter, to remove the singularity from equation (9b), the statement in the denominator of this equation is expressed as a factor of $A_0 - Z$ as follows:

$$E^{(\mathrm{tot})}(A_0) - E^{(\mathrm{tot})}(Z) = (A_0 - Z)H^{(\mathrm{tot})}(Z), \tag{10}$$

where $H^{(\mathrm{tot})}(Z)\big|_{Z=A_0} \neq 0$.

Since the total potential energy consists of vdW and electrostatic energies, $H^{(\mathrm{tot})}(Z)$ can be written as:

$$H^{(\mathrm{tot})}(Z) = H^{(\mathrm{vdW})}(Z) + H^{(\mathrm{elec})}(Z). \tag{11}$$

After an extensive mathematical manipulation, $H^{(\mathrm{vdW})}(Z)$ and $H^{(\mathrm{elec})}(Z)$ are derived as:

$$H^{(\mathrm{vdW})}(Z) = \sum_{n=1}^{2}\left(\Gamma_n\left(\frac{1}{1+\zeta_n\vartheta_n} - \frac{(\zeta_n-\vartheta_n)^2}{3(1+\zeta_n\vartheta_n)^3}\right) + \sum_{i=1}^{5}\sum_{j=0}^{i}\Gamma_{nij}\frac{\vartheta_n^{2j} + \zeta_n^{2j} - \sum_{k=1}^{2j+1}\vartheta_n^{2j-k+1}\zeta_n^{k-1}}{\left(1+\zeta_n^2\right)^i\left(1+\vartheta_n^2\right)^i}\right), \tag{12a}$$

$$H^{(\mathrm{elec})}(Z) = -\sum_{n=1}^{2}\frac{kq\,Q(\vartheta_n+\zeta_n)}{R_c^2\left(\left(1+\vartheta_n^2\right)\sqrt{1+\zeta_n^2}+\left(1+\zeta_n^2\right)\sqrt{1+\vartheta_n^2}\right)}, \tag{12b}$$

in which $\zeta_n = \dfrac{A_{0_n}}{R_c}$; $A_{0_1} = A_0 + L$, $A_{0_2} = A_0 - L$ and

$$\Gamma_n = (-1)^{n+1}\frac{G_1}{R_c}, \quad \Gamma_{nij} = (-1)^{n+1}\frac{G_{2i-1}\binom{i}{j}}{R_c}. \tag{13}$$

The detailed derivation of equation (12) is presented in Appendix.

Now, making the substitution of equation (10) with equation (9b) and then, deriving $Z = A_0\sin^2\varphi$, one can arrive at:

$$T_2 = 2\alpha\sqrt{2m_I A_0}\int_{\sin^{-1}\sqrt{\delta}}^{\pi/2}\frac{\sin\varphi}{\sqrt{H^{(\mathrm{tot})}(Z)}}\mathrm{d}\varphi. \tag{14}$$

Finally, the period of motion is achieved through summing up equations (9a) and (14) and then, the oscillation frequency is obtained as the reciprocal of the period of motion.

4. Numerical results and discussion

Based on the semi-analytical expression proposed for the oscillation frequency, a detailed parametric study is conducted herein to gain an insight into the effects of different parameters such as sign and magnitude of functional group charge, nanotube length, initial separation distance and initial velocity on the dynamic behaviour of chloride ion-electrically charged CNT oscillators. The results are also compared with the ones when the functional groups are removed.

To ascertain the accuracy and efficiency of the proposed frequency formula, a comparison is made between the frequency results obtained from the energy and motion equations. The frequency–amplitude curves related to $C = -0.1,\ \ 0.1$ and 0 are generated from these equations and are compared and shown in figure 3. This figure confirms that the frequencies predicted by semi-analytical and numerical solutions are in reasonable agreement. According to the discussion presented earlier in figure 2, for the positive value of the parameter C, the frequency–amplitude curves related to the first and second oscillatory zones are shown separately in figure 3a and b, respectively. The results of the first zone are compared with the ones corresponding to negatively charged and uncharged CNTs. The results of the second zone, however, are only compared with the ones corresponding to uncharged CNTs due to the limitation on the motion amplitude for negatively charged CNTs. As demonstrated, the frequency curve against the amplitude is monotonically decreasing in the first zone, whereas in the second zone, has a peak rather than a monotonic behaviour. From figure 3a, the highest frequency in the first zone of $C = 0.1$ is obtained as 317.8 GHz which is 6 and 8.14 times higher than those of $C = -0.1$ and 0, respectively. In contrast, from figure 3b, the maximum frequency in the second zone of $C = 0.1$ is calculated as 32.19 GHz which is 0.82 times lower than that of $C = 0$. Thus, one can deduce that the optimal frequency is achieved when the chloride ion oscillates near the ends of a positively charged CNT. Closer inspection to figure 3b also reveals that when the amplitude of motion is equal to 66.45 Å, the frequencies obtained in the cases of $C = 0$ and 0.1 reach the same value of 31.06 GHz. For the amplitudes lower than 66.45 Å, higher frequencies are produced in the case of $C = 0$, while for the amplitudes higher than 66.45 Å, greater frequencies are generated in the case of $C = 0.1$.

4.1 *Oscillation of the chloride ion inside negatively charged CNTs*

In this subsection, the oscillatory behaviour of the chloride ion inside negatively charged CNTs is investigated. The effect of functional group charge on the variations of frequency with the amplitude, initial velocity with the amplitude and frequency with the initial velocity is respectively studied and is shown in figure 4a–c and the corresponding results are compared with the ones related to an uncharged CNT. In figure 4a, it is assumed that the ion is initially at rest and starts its oscillatory motion with an initial separation distance. In figure 4c, however, it is assumed that the ion possesses an initial velocity at the preferred position of the system which occurs at the middle length of the nanotube. It is worth mentioning that these curves are plotted until the point where the oscillatory motion

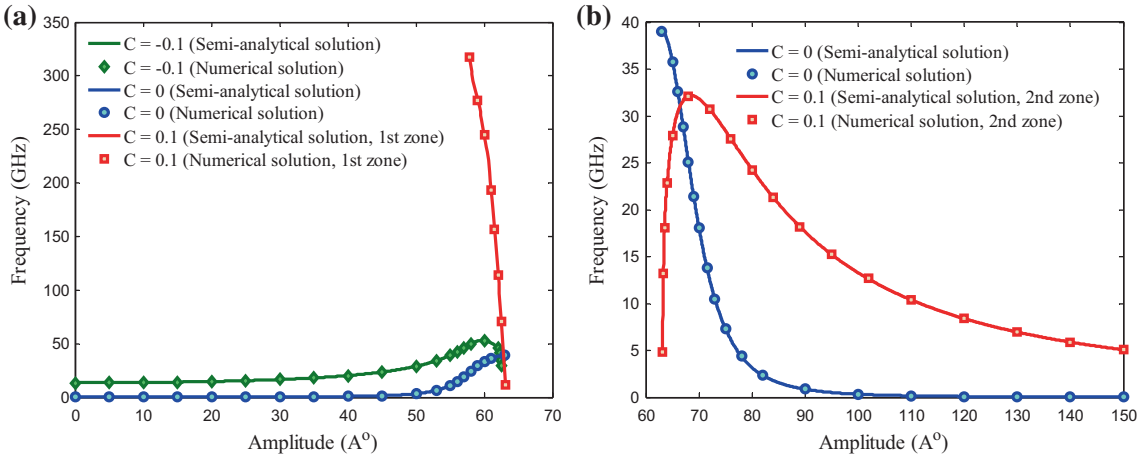

Figure 3. Comparison of frequency–amplitude curves obtained from energy and motion equations corresponding to **(a)** negatively charged, positively charged (first zone) and uncharged CNTs and **(b)** uncharged and positively charged (second zone) CNTs $(L = 60\,\text{Å})$.

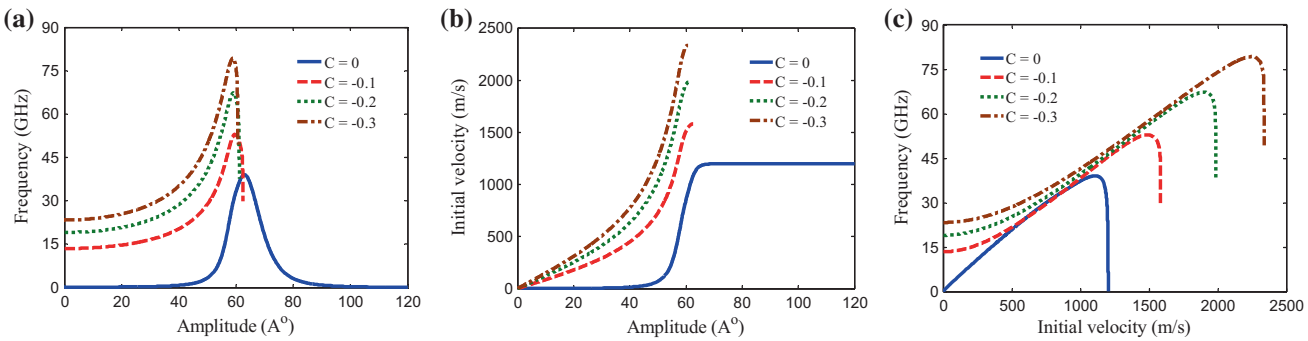

Figure 4. **(a)** Frequency against amplitude, **(b)** initial velocity against amplitude and **(c)** frequency against initial velocity corresponding to uncharged and negatively charged CNTs $(L = 60\,\text{Å})$.

can occur. From figure 4a, in the absence and presence of functional groups, the frequency curves are shown to have a peak. The highest value of frequency and the associated amplitude are called as the maximum frequency and critical amplitude, respectively. For a given amplitude, it is seen that increasing the magnitude of the parameter C leads to increase in the oscillation frequency. According to figure 4b, the initial velocity curves associated with negatively charged CNTs are monotonically rising, while that related to an uncharged CNT reaches a plateau. This figure also reveals that decorating both ends of the nanotube with functional groups having more negative electric charges intensifies the ultimate value of the initial velocity. Like frequency–amplitude curves, frequency–initial velocity curves reach a climax at a special velocity called as the critical velocity. In addition, for a given initial velocity, higher frequencies are produced for higher magnitudes of the parameter C.

Figure 5a–c shows how the critical amplitude, critical velocity and maximum frequency, respectively, vary with the parameter C in the cases of negatively charged and uncharged CNTs. It can be observed that the critical amplitude decreases gradually, while the critical velocity and the maximum frequency increase considerably as the magnitude of the parameter C increases. It can be further observed that the critical amplitude occurs in the vicinity of the nanotube right end. In the absence of functional groups, this amplitude takes place outside the nanotube and moves towards the inside of the nanotube by increasing the magnitude of functional group charge.

The variations of frequency with the amplitude, initial velocity with the amplitude and frequency with the amplitude corresponding to different lengths of a negatively charged CNT are presented in figure 6a–c, respectively. It can be seen that the global shapes of these curves are not affected by the length of the nanotube, whereas the critical amplitude, critical velocity and maximum frequency vary with the nanotube length. For a given initial condition, it can be almost concluded that the ion oscillates with higher frequencies inside shorter nanotubes. Moreover, enlarging the nanotube length leads to decrease in the initial velocity for a given

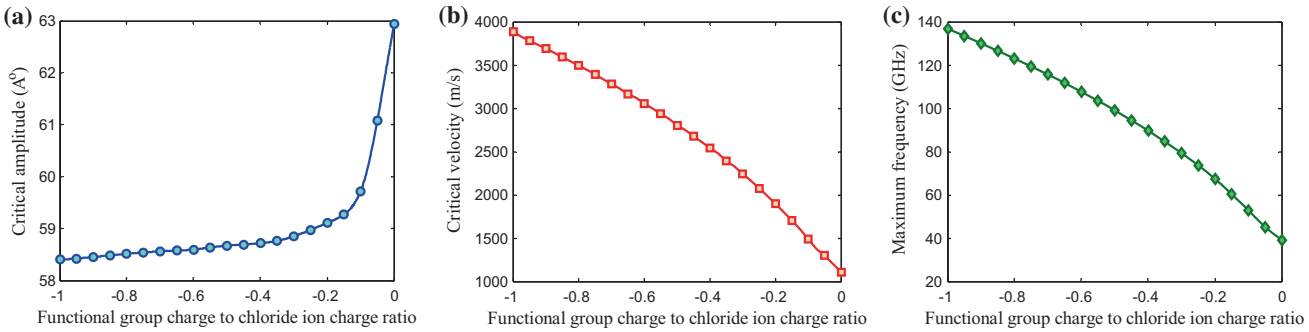

Figure 5. **(a)** Critical amplitude, **(b)** critical velocity and **(c)** maximum frequency corresponding to uncharged and negatively charged CNTs $(L = 60\,\text{Å})$.

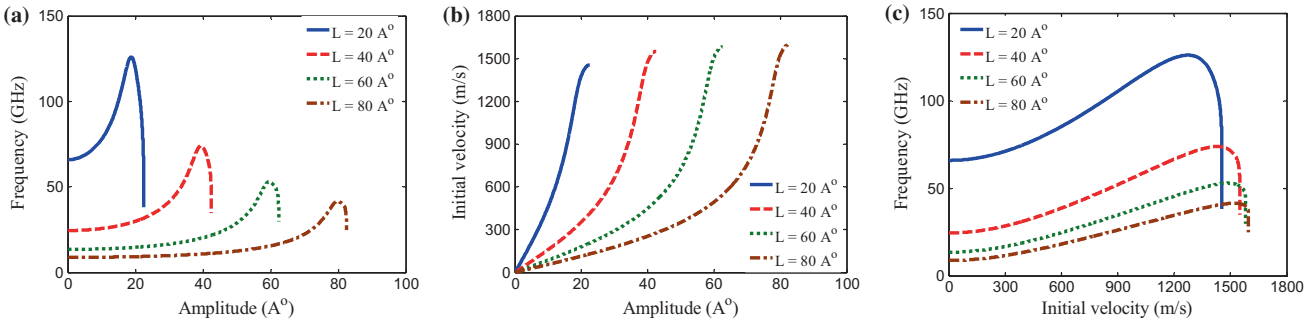

Figure 6. **(a)** Frequency against amplitude, **(b)** initial velocity against amplitude and **(c)** frequency against initial velocity associated with different lengths of CNTs ($C = -0.1$).

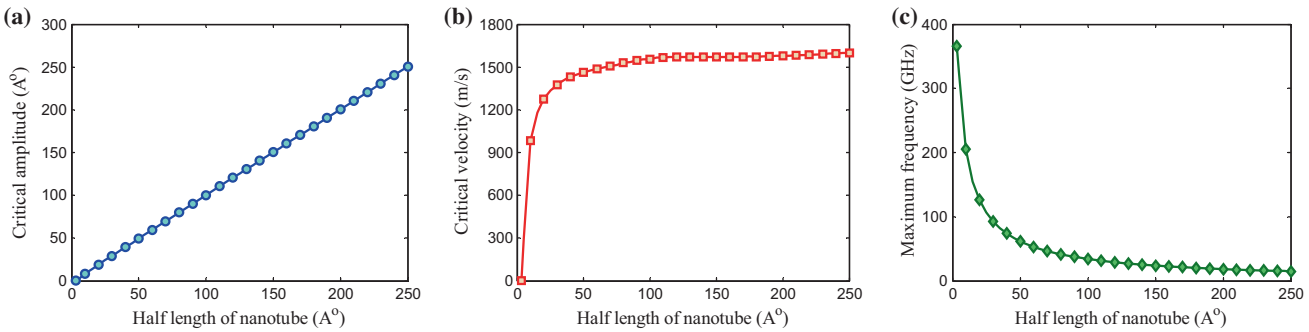

Figure 7. **(a)** Critical amplitude, **(b)** critical velocity and **(c)** maximum frequency associated with different lengths of CNTs ($C = -0.1$).

amplitude. By contrast, the ultimate value of the initial velocity is shown to increase as the nanotube length becomes larger and such an increase is more pronounced for shorter nanotubes.

The effect of the nanotube length on the critical amplitude, critical velocity and maximum frequency associated with a negatively charged CNT is investigated in figure 7a–c, respectively. It is found that the critical amplitude increases linearly with the half-length of the nanotube according to $A_c = 1.009L - 1.223$. It is also shown that the critical velocity increases, while the maximum frequency decreases as the nanotube length becomes larger and this behaviour is more noticeable for shorter nanotubes.

4.2 *Oscillation of chloride ion inside positively charged CNTs*

In this subsection, the oscillatory behaviour of the chloride ion inside positively charged CNTs is studied. In accordance with the discussion previously presented in figure 3, the numerical results of this case are provided for both first and second oscillatory zones at which the core respectively oscillates near the right end of the nanotube and with respect to its middle length. For both the first and second zones, the variations of frequency with the amplitude, initial velocity with the amplitude and frequency with the initial velocity corresponding to different values of the parameter C are illustrated in figure

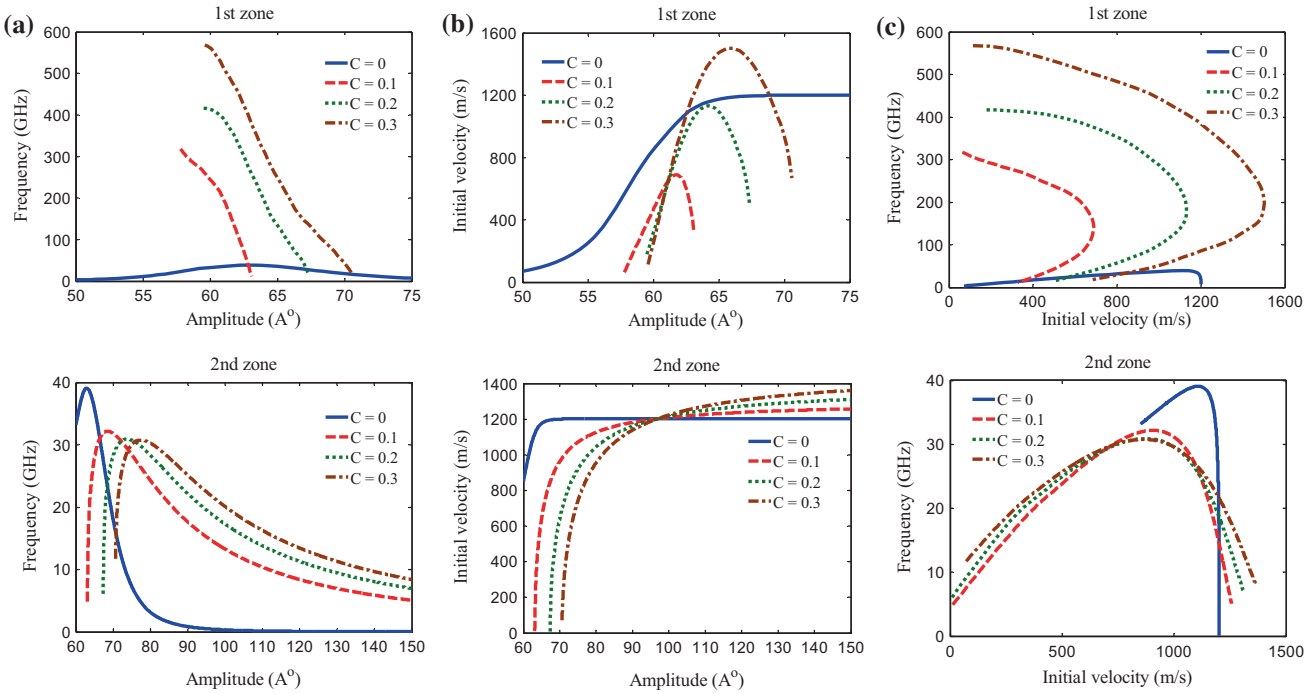

Figure 8. **(a)** Frequency *vs*. amplitude, **(b)** initial velocity *vs*. amplitude and **(c)** frequency *vs*. initial velocity obtained in the first and second oscillatory zones related to uncharged and positively charged CNTs $(L = 60\,\text{Å})$.

8a–c, respectively. For comparison purposes, the results related to an uncharged CNT are also presented. According to this figure, one can observe that the overall shapes of frequency–amplitude, initial velocity–amplitude and frequency–initial velocity curves in the first zone are totally different from those in the second zone. In the first zone, it can be seen that the increase in the charges of functional groups leads to a considerable increase in the oscillation frequency, if the amplitude is remained constant. In the second zone, however, this behaviour is true only for a specific range of amplitude. From figure 8b, the initial velocity–amplitude curves in the first zone have a peak, while those in the second zone behave increasingly and tend to approach their asymptote value for sufficiently large amplitudes. The ultimate values of the initial velocities predicted in both the zones are shown to increase with enlarging the charges of functional groups. This figure also reveals that there exists a special amplitude at which the initial velocity is invariable regardless of the magnitude of electric charges and this finding is true for both the zones. This initial velocity and the corresponding amplitude are termed as invariable velocity and invariable amplitude, respectively. In the first and second zones, the invariable amplitude and invariable velocity are obtained as 61.17 Å, 669.5 ms^{-1} and 96.96 Å, 1202 ms^{-1}, respectively. For the amplitudes lower than the invariable one, higher initial velocities are obtained for lower electric charges of functional groups. For the amplitudes higher than the invariable one, however, higher initial velocities are obtained for higher electric charges of functional groups. As depicted in figure 8c, a parabolic-like behaviour can be observed for frequency–initial velocity curves, so that they open left in the first zone, while they open down in the second zone. It can be further observed that the turning point of frequency–initial velocity curves considerably shifts to the right in the first zone, while it gradually shifts to the down in the second zone as the parameter C increases. In the second zone, one can also detect two invariable points; the first and the second invariable points relate to 709.9 ms^{-1}, 29.65 GHz and 1079 ms^{-1}, 27.55 GHz, respectively. For the initial velocities lower than the first invariable velocity and higher than the second invariable velocity, frequency is shown to increase by enlarging the electric charges of functional groups.

For both first and second oscillatory zones, figure 9a–c are respectively presented to show how the critical amplitude, critical velocity and maximum frequency vary with the parameter C in the cases of positively charged and uncharged CNTs. In the first zone, it can be observed that the critical amplitude reaches its lowest value of 57.4 Å at $C = 0.07$ and also it changes gradually for $C \geq 0.14$. In contrast, the critical amplitude curve against the parameter C is monotonically increasing in the second zone. From figure 9b, the critical velocity is shown to vary non-uniformly with the parameter 'C' in the first zone. In this case, for $0 < C < 0.621$, the critical velocity has two local minima $\left((0.089, 48.4\,\text{ms}^{-1}), (0.29, 113.2\,\text{ms}^{-1})\right)$ and one local maximum $(0.154, 237.1\,\text{ms}^{-1})$; for $0.621 < C < 0.884$, the critical velocity gradually decreases and for

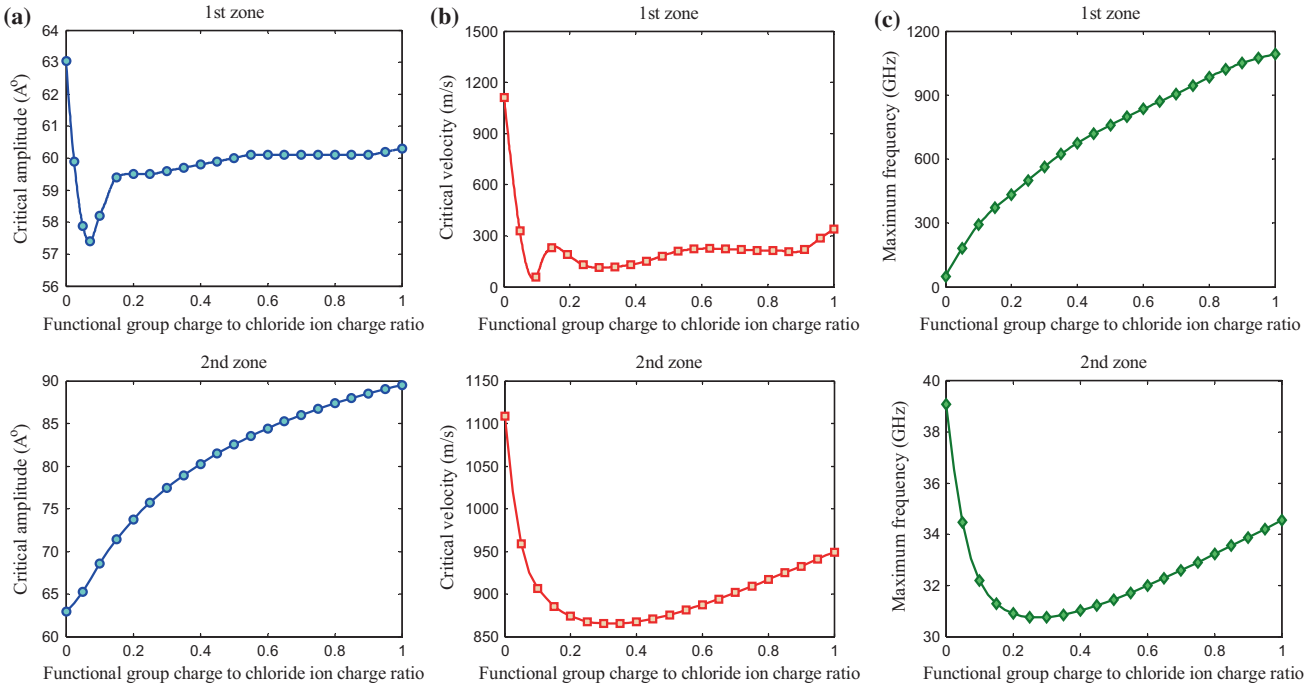

Figure 9. **(a)** Critical amplitude, **(b)** critical velocity and **(c)** maximum frequency obtained in the first and second oscillatory zones related to uncharged and positively charged CNTs $(L = 60\,\text{Å})$.

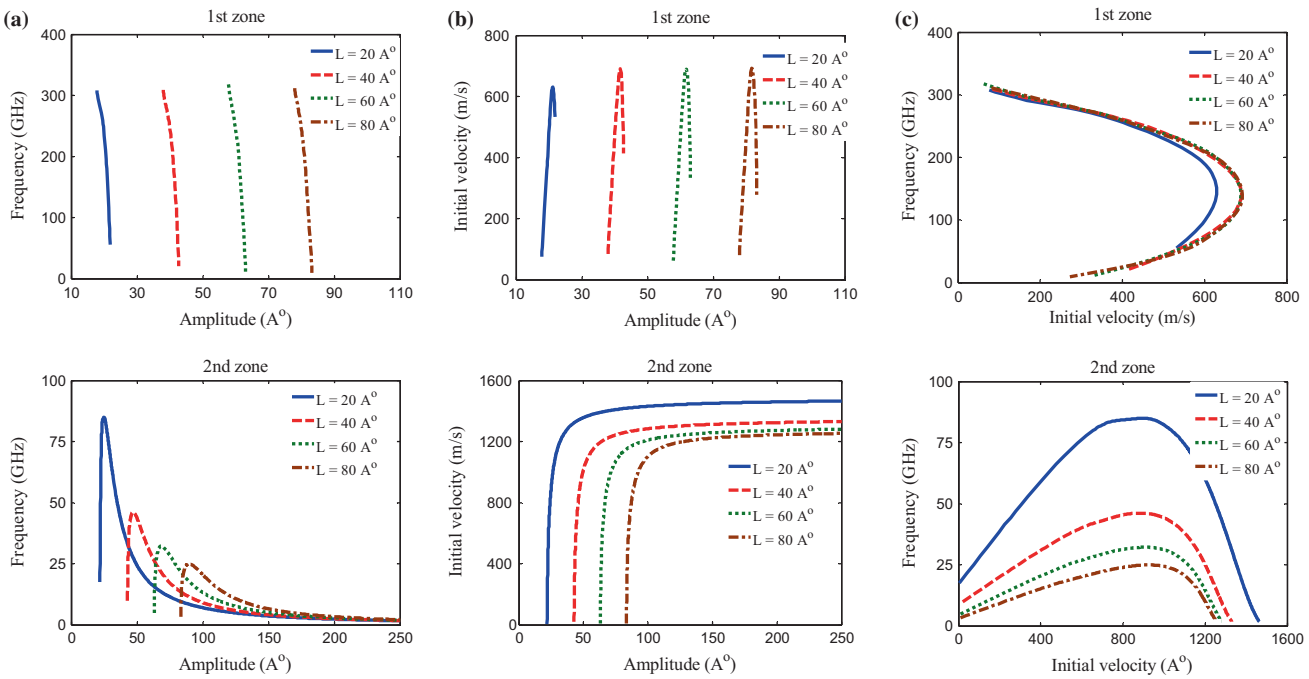

Figure 10. **(a)** Frequency *vs*. amplitude, **(b)** initial velocity *vs*. amplitude and **(c)** frequency *vs*. initial velocity obtained in the first and second oscillatory zones associated with different lengths of CNTs ($C = 0.1$).

$C > 0.884$, the critical velocity shows rising behaviour. In the second zone, however, the critical velocity has a local minimum $(0.325, 865.3\,\text{ms}^{-1})$ and after that it shows increasing behaviour. Figure 9c also reveals that the maximum frequency curve *vs*. parameter C is monotonically rising in the first zone. In contrast, in the second zone, the maximum frequency curve shows similar behaviour to the critical velocity curve as the parameter C changes. In this case, the lowest

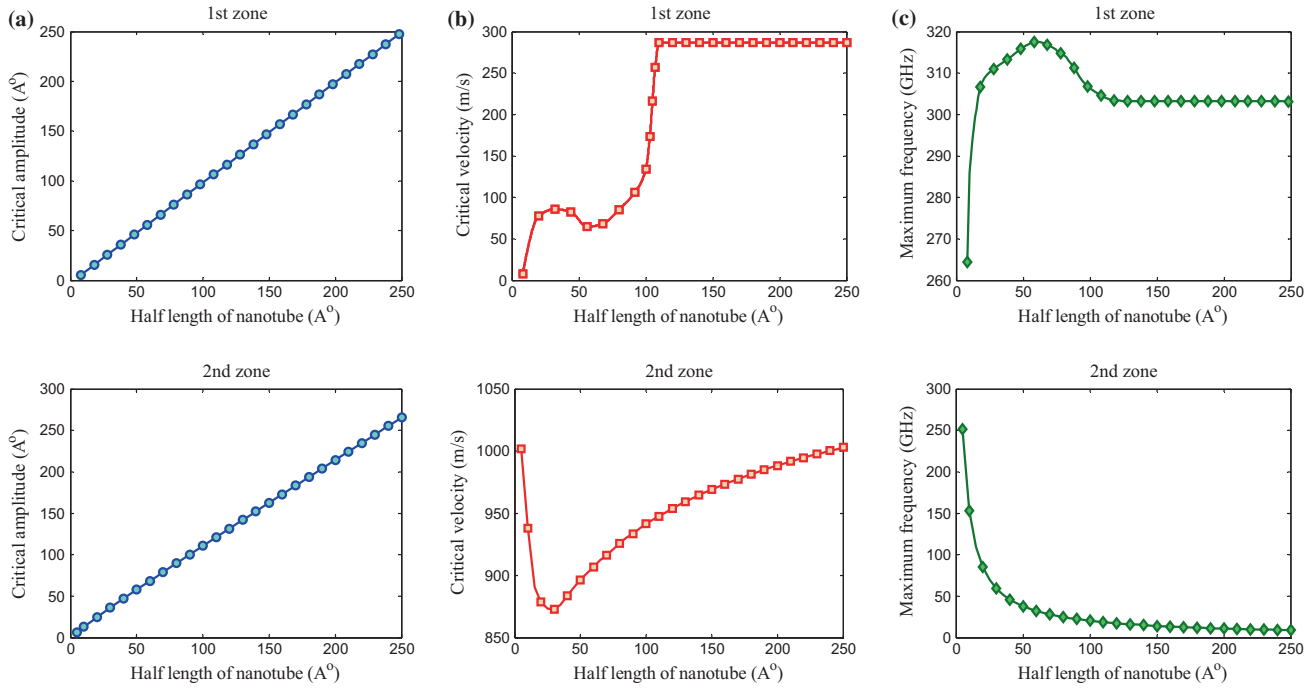

Figure 11. **(a)** Critical amplitude, **(b)** critical velocity and **(c)** maximum frequency obtained in the first and second oscillatory zones associated with different lengths of CNTs ($C = 0.1$).

frequency is obtained as 30.75 GHz which corresponds to $C = 0.275$.

The variations in frequency with the amplitude, initial velocity with the amplitude and frequency with the initial velocity associated with different lengths of a positively charged CNT are respectively shown in figure 10a–c for both the oscillatory zones. Similar to figure 6, it can be seen that the overall shapes of these figures are not influenced by the length of the nanotube. As depicted, frequency–amplitude curves shift to the right by enlarging the nanotube length. Furthermore, in the first and second zones, the ultimate value of the initial velocity decreases by enlarging the nanotube length. Compared to the first zone, the frequency–initial velocity curve of the second zone is found to be more affected by the length of the nanotube. In this zone, for a given initial velocity, shorter nanotubes yield greater frequencies.

Considering a positively charged CNT, the effect of the nanotube length on the critical amplitude, critical velocity and maximum frequency is respectively highlighted in figure 11a–c for both the oscillatory zones. Based on the computed results, it is found that the critical amplitude varies linearly with respect to the half-length of the nanotube in the first and second zones according to $A_c = 1.008L - 2.553$ and $A_c = 1.047L + 5.119$, respectively. In the first zone, the critical velocity curve has a local maximum $(32.4\,\text{Å}, 85.88\ \text{ms}^{-1})$ and a local minimum $(56.3\,\text{Å}, 64.57\,\text{ms}^{-1})$ and it remains constant at the value of $286.7\,\text{ms}^{-1}$ for $L \geq 110\,\text{Å}$. In the second zone, however, the critical velocity curve has a local minimum $(30\,\text{Å}, 872.6\,\text{ms}^{-1})$ and after this point, it shows increasing behaviour. In addition, the maximum frequency of the first zone reaches the highest value of 317.4 GHz at $L = 58\,\text{Å}$ and then shows a decreasing behaviour to reach a constant value of 303.2 GHz for $L \geq 118\,\text{Å}$. In contrast, the maximum frequency of the second zone decreases with enlarging the nanotube length and this reduction is more considerable for shorter nanotubes.

5. Conclusion

The dynamic behaviour of nano-oscillators based on the chloride ion inside functionalized CNTs was studied using a continuum approach. Employing the conservation of mechanical energy principle, a novel semi-analytical expression was proposed for the precise evaluation of oscillation frequency. To ascertain the accuracy and validity of the proposed frequency formula, frequencies predicted from the energy equation were compared with the ones obtained from the motion equation. Based on the frequency expression, a detailed parametric study on different aspects of operating frequencies under various system parameters such as sign and magnitude of functional group charge, nanotube length and initial conditions was performed which revealed some fresh insights into the problem. For both negatively charged and uncharged CNTs, it was found that the chloride ion has one preferred position taking place at the middle length of the nanotube. In the case of positively charged CNTs, however, two oscillatory zones, namely first and second zones, were distinguished at

which the ion oscillates with respect to the middle length and near the ends of the nanotube, respectively. In this case, it was observed that the frequencies produced in the first zone are considerably higher than those produced in the second zone. The overall shapes of frequency response curves were shown to be affected only by the sign of electric charges. Moreover, frequency curves obtained in the first and second oscillatory zones of positively charged CNTs were found to have different shapes. The critical conditions and the corresponding maximum frequencies were obtained and their strong dependence on the sign and magnitude of electric charges and nanotube length was observed. In the case of negatively charged CNTs, it was demonstrated that the maximum frequency increases as the magnitude of electric charge increases, while it decreases, especially for shorter nanotubes, as the length of the nanotube enlarges. In the case of positively charged CNTs and in the first oscillatory zone, it was also observed that the maximum frequency increases monotonically as electric charges increase, whereas it tends to reach a constant value for sufficiently long nanotubes. Moreover, in the second oscillatory zone, it was shown that there exists a value for electric charge beyond which the maximum frequency curve behaves monotonically rising, whereas the behaviour of the maximum frequency against the length of the nanotube is decreasing especially, for shorter nanotubes.

Appendix

According to equation (2), vdW potential energy is composed of two terms as:

$$E_1^{(\mathrm{vdW})}(Z) = \sum_{n=1}^{2}(-1)^{n+1}G_1 \tan^{-1}\vartheta_n, \tag{A1}$$

$$E_2^{(\mathrm{vdW})}(Z) = \sum_{n=1}^{2}\sum_{i=1}^{5}(-1)^{n+1}G_{2i-1}\frac{\vartheta_n}{\left(1+\vartheta_n^2\right)^i}. \tag{A2}$$

Using equation (A1), one can write:

$$E_1^{(\mathrm{vdW})}(A_0) - E_1^{(\mathrm{vdW})}(Z) = \sum_{n=1}^{2}(-1)^{n+1}G_1\left(\tan^{-1}\zeta_n - \tan^{-1}\vartheta_n\right). \tag{A3}$$

Applying a trigonometric identity to the expression given in the parenthesis of the prior equation leads to:

$$\tan^{-1}\zeta_n - \tan^{-1}\vartheta_n = \tan^{-1}\left(\frac{\zeta_n-\vartheta_n}{1+\zeta_n\vartheta_n}\right). \tag{A4}$$

Employing a Taylor series expansion for equation (A4) and then, substituting the resulting expression into equation (A3), one can arrive at:

$$E_1^{(\mathrm{vdW})}(A_0) - E_1^{(\mathrm{vdW})}(Z) = (A_0 - Z)H_1^{(\mathrm{vdW})}(Z), \tag{A5}$$

in which

$$H_1^{(\mathrm{vdW})}(Z) = \sum_{n=1}^{2}\Gamma_n\left(\frac{1}{1+\zeta_n\vartheta_n} - \frac{(\zeta_n-\vartheta_n)^2}{3(1+\zeta_n\vartheta_n)^3}\right). \tag{A6}$$

Using equation (A2), one can also write:

$$E_2^{(\mathrm{vdW})}(A_0) - E_2^{(\mathrm{vdW})}(Z) = \sum_{n=1}^{2}\sum_{i=1}^{5}(-1)^{n+1}G_{2i-1} \times\left(\frac{\zeta_n\left(1+\vartheta_n^2\right)^i - \vartheta_n\left(1+\zeta_n^2\right)^i}{\left(1+\zeta_n^2\right)^i\left(1+\vartheta_n^2\right)^i}\right). \tag{A7}$$

The numerator of equation (A7) utilizing the Khayyam's binomial expansion can be reformulated as follows:

$$\zeta_n\left(1+\vartheta_n^2\right)^i - \vartheta_n\left(1+\zeta_n^2\right)^i = \sum_{j=0}^{i}\binom{i}{j}((\zeta_n-\vartheta_n)\left(\vartheta_n^{2j}+\zeta_n^{2j}\right) + \vartheta_n^{2j+1} - \zeta_n^{2j+1}). \tag{A8}$$

Based on the following relation:

$$\vartheta_n^{2j+1} - \zeta_n^{2j+1} = -(\zeta_n-\vartheta_n)\sum_{k=1}^{2j+1}\vartheta_n^{2j-k+1}\zeta_n^{k-1}. \tag{A9}$$

Equation (A8) is rewritten as a factor of $\zeta_n - \vartheta_n$ as:

$$\zeta_n\left(1+\vartheta_n^2\right)^i - \vartheta_n\left(1+\zeta_n^2\right)^i = (\zeta_n-\vartheta_n)\sum_{j=0}^{i}\binom{i}{j} \times\left(\vartheta_n^{2j} + \zeta_n^{2j} - \sum_{k=1}^{2j+1}\vartheta_n^{2j-k+1}\zeta_n^{k-1}\right). \tag{A10}$$

Thus, on making the substitution of equation (A10) with equation (A7), one can have:

$$E_2^{(\mathrm{vdW})}(A_0) - E_2^{(\mathrm{vdW})}(Z) = (A_0 - Z)H_2^{(\mathrm{vdW})}(Z), \tag{A11}$$

where

$$H_2^{(\mathrm{vdW})}(Z) = \sum_{n=1}^{2}\sum_{i=1}^{5}\sum_{j=0}^{i}\Gamma_{nij}\frac{\vartheta_n^{2j} + \zeta_n^{2j} - \sum_{k=1}^{2j+1}\vartheta_n^{2j-k+1}\zeta_n^{k-1}}{\left(1+\zeta_n^2\right)^i\left(1+\vartheta_n^2\right)^i}. \tag{A12}$$

Finally, summing up equation (A6) and equation (A12), $H^{(\mathrm{vdW})}(Z)$ is derived as:

$$H^{(\mathrm{vdW})}(Z)=\sum_{n=1}^{2}\left(\Gamma_n\left(\frac{1}{1+\zeta_n\vartheta_n}-\frac{(\zeta_n-\vartheta_n)^2}{3(1+\zeta_n\vartheta_n)^3}\right)+\sum_{i=1}^{5}\sum_{j=0}^{i}\Gamma_{nij}\frac{\vartheta_n^{2j}+\zeta_n^{2j}-\sum_{k=1}^{2j+1}\vartheta_n^{2j-k+1}\zeta_n^{k-1}}{\left(1+\zeta_n^2\right)^i\left(1+\vartheta_n^2\right)^i}\right). \tag{A13}$$

Moreover, using electrostatic energy given in equation (4), one can write:

$$E^{(\mathrm{elec})}(A_0)-E^{(\mathrm{elec})}(Z)=\sum_{n=1}^{2}\frac{kqQ}{R_\mathrm{c}}\left(\frac{(\vartheta_n-\zeta_n)(\vartheta_n+\zeta_n)}{\left(1+\vartheta_n^2\right)\sqrt{1+\zeta_n^2}+\left(1+\zeta_n^2\right)\sqrt{1+\vartheta_n^2}}\right). \tag{A14}$$

This equation can be reformulated as a factor of A_0-Z as follows:

$$E^{(\mathrm{elec})}(A_0)-E^{(\mathrm{elec})}(Z)=(A_0-Z)H^{(\mathrm{elec})}(Z) \tag{A15}$$

in which

$$H^{(\mathrm{elec})}(Z)=-\sum_{n=1}^{2}\frac{kqQ(\vartheta_n+\zeta_n)}{R_\mathrm{c}^2\left(\left(1+\vartheta_n^2\right)\sqrt{1+\zeta_n^2}+\left(1+\zeta_n^2\right)\sqrt{1+\vartheta_n^2}\right)}. \tag{A16}$$

References

[1] Lee S W and Campbell E E 2013 *Curr. Appl. Phys.* **13** 1844
[2] Natsuki T, Matsuyama N, Shi J X and Ni Q Q 2014 *Appl. Phys. A* **116** 1001
[3] Damnjanović M, Milošević I, Vuković T and Sredanović R 1999 *Phys. Rev. B* **60** 2728
[4] Tuzun R E, Noid D W and Sumpter B G 1995 *Nanotechnology* **6** 64
[5] Eichler A, Chaste J, Moser J and Bachtold A 2011 *Nano Lett.* **11** 2699
[6] Shadmani P, Montazeri A, Taherifar N and Motevalli B 2017 *Int. J. Mech. Sci.* **121** 187
[7] Liu P, Zhang Y W and Lu C 2005 *J. Appl. Phys.* **97** 094313
[8] Hilder T A and Hill J M 2007 *Micro & Nano Lett.* **2** 50
[9] Ansari R, Sadeghi F and Ajori S 2017 *Eur. J. Mech. A Solids* **62** 67
[10] Cumings J and Zettl A 2000 *Science* **289** 602
[11] Zheng Q and Jiang Q 2002 *Phys. Rev. Lett.* **88** 045503
[12] Zheng Q, Liu J Z and Jiang Q 2002 *Phys. Rev. B* **65** 245409
[13] Roukes M 2001 *Phys. World* **14** 25
[14] Blencowe M P and Wybourne M N 2000 *Appl. Phys. Lett.* **77** 3845
[15] Gevorgyan T V, Shahinyan A R and Kryuchkyan G Y 2012 *Phys. Rev. A* **85** 053802
[16] Beck G M and Sergi A 2013 *Phys. Lett. A* **377** 1047
[17] Photiadis D M, Bucaro J A and Liu X 2006 *Phys. Rev. B* **73** 165314
[18] Po G and Ghoniem N M 2010 *J. Appl. Phys.* **107** 094310
[19] Kang J W, Kim K S, Hwang H J and Kwon O K 2010 *Phys. Lett. A* **374** 3658
[20] Zhao X and Cummings P T 2006 *J. Chem. Phys.* **124** 134705
[21] Kang J W, Song K O, Hwang H J and Jiang Q 2006 *Nanotechnology* **17** 2250
[22] Su H, Goddard III W A and Zhao Y 2006 *Nanotechnology* **17** 5691
[23] Legoas S B, Coluci V R, Braga S F, Coura P Z, Dantas S O and Galvão D S 2003 *Phys. Rev. Lett.* **90** 055504
[24] Legoas S B, Coluci V R, Braga S F, Coura P Z, Dantas S O and Galvão D S 2004 *Nanotechnology* **15** S184
[25] Rivera J L, McCabe C and Cummings P T 2003 *Nano Lett.* **3** 1001
[26] Rivera J L, McCabe C and Cummings P T 2004 *Nanotechnology* **16** 186
[27] Liu P, Zhang Y W and Lu C 2005 *J. Appl. Phys.* **98** 014301
[28] Coluci V R, Legoas S B, De Aguiar M A M and Galvão D S 2005 *Nanotechnology* **16** 583
[29] Song H Y and Zha X W 2009 *Phys. Lett. A* **373** 1058
[30] Ansari R, Ajori S and Sadeghi F 2015 *J. Phys. Chem. Solids* **85** 264
[31] Zhao Y, Ma C C, Chen G and Jiang Q 2003 *Phys. Rev. Lett.* **91** 175504
[32] Guo W, Guo Y, Gao H, Zheng Q and Zhong W 2003 *Phys. Rev. Lett.* **91** 125501
[33] Servantie J and Gaspard P 2006 *Phys. Rev. B* **73** 125428
[34] Sadeghi F, Ansari R and Darvizeh M 2015 *Eur. Phys. J. D* **69** 285
[35] Baowan D, Thamwattana N and Hill J M 2007 *Eur. Phys. J. D* **44** 117
[36] Sadeghi F and Ansari R 2017 *Eur. Phys. J. Plus* **132** 309
[37] Girifalco L A 1991 *J. Phys. Chem.* **95** 5370
[38] Girifalco L A 1992 *J. Phys. Chem.* **96** 858
[39] Girifalco L A 1995 *Phys. Rev. B* **52** 9910
[40] Hodak M and Girifalco L A 2001 *Chem. Phys. Lett.* **350** 405
[41] Hilder T A and Hill J M 2008 *Micro & Nano Lett.* **3** 18
[42] Chan Y and Hill J M 2011 *Nanoscale Res. Lett.* **6** 203
[43] Chan Y and Hill J M 2012 *Eur. Phys. J. B* **85** 56
[44] Ansari R and Sadeghi F 2012 *J. Nanotechnol. Eng. Med.* **3** 011001
[45] Zavalniuk V and Marchenko S 2011 *Low Temp. Phys.* **37** 337
[46] Baowan D and Hill J M 2007 *Z. Angew. Math. Phys.* **58** 857
[47] Cox B J, Thamwattana N and Hill J M 2006 *Proc. R. Soc. London, Ser. A* **463** 477
[48] Thamwattana N, Cox B J and Hill J M 2009 *J. Phys.: Condens. Matter* **21** 144214
[49] Ansari R and Motevalli B 2011 *J. Vib. Acoust.* **133** 051003
[50] Ansari R, Sadeghi F and Motevalli B 2013 *Commun. Nonlinear Sci. Numer. Simul.* **18** 769
[51] Ansari R, Alipour A and Sadeghi F 2012 *J. Appl. Phys.* **112** 124310
[52] Ansari R, Sadeghi F and Alipour A 2013 *J. Vib. Acoust.* **135** 051009
[53] Zubair A, Tristant D, Nie C, Tsentalovich D E, Headrick R J, Pasquali M *et al* 2017 *Phys. Rev. Materi.* **1** 064002
[54] Chan Y and Hill J M 2013 *J. Math. Chem.* **51** 1258
[55] Sadeghi F, Ansari R and Darvizeh M 2016 *Physica E* **80** 69